Molecular Systems Biology 8; Article number 616; doi:10.1038/msb.2012.46
Citation: ***Molecular Systems Biology*** **8:616**

www.molecularsystemsbiology.com

molecular systems biology

Need-based activation of ammonium uptake in *Escherichia coli*

Minsu Kim[1], Zhongge Zhang[2], Hiroyuki Okano[1], Dalai Yan[3], Alexander Groisman[1,*] and Terence Hwa[1,2,4,*]

[1] Department of Physics, University of California at San Diego, La Jolla, CA, USA, [2] Section of Molecular Biology, Division of Biological Sciences, University of California at San Diego, La Jolla, CA, USA, [3] Department of Microbiology and Immunology, Indiana University School of Medicine, Indianapolis, IN, USA and [4] Center for Theoretical Biological Physics, University of California at San Diego, La Jolla, CA, USA

* Corresponding authors. T Hwa or A Groisman, Department of Physics, University of California at San Diego, 9500 Gilman Drive, La Jolla, CA 92093-0374, USA. Tel.: +1 858 534 7263; Fax: +1 858 534 7697; E-mail: hwa@ucsd.edu or Tel.: +1 858 822 1838; Fax: +1 858 534 7697; E-mail: agroisman@ucsd.edu

Received 4.6.12; accepted 15.8.12

The efficient sequestration of nutrients is vital for the growth and survival of microorganisms. Some nutrients, such as CO_2 and NH_3, are readily diffusible across the cell membrane. The large membrane permeability of these nutrients obviates the need of transporters when the ambient level is high. When the ambient level is low, however, maintaining a high intracellular nutrient level against passive back diffusion is both challenging and costly. Here, we study the delicate management of ammonium (NH_4^+/NH_3) sequestration by *E. coli* cells using microfluidic chemostats. We find that as the ambient ammonium concentration is reduced, *E. coli* cells first maximize their ability to assimilate the gaseous NH_3 diffusing into the cytoplasm and then abruptly activate ammonium transport. The onset of transport varies under different growth conditions, but always occurring just as needed to maintain growth. Quantitative modeling of known interactions reveals an integral feedback mechanism by which this need-based uptake strategy is implemented. This novel strategy ensures that the expensive cost of upholding the internal ammonium concentration against back diffusion is kept at a minimum.
Molecular Systems Biology **8:** 616; published online 25 September 2012; doi:10.1038/msb.2012.46
Subject Categories: metabolic and regulatory networks; simulation and data analysis; cellular metabolism
Keywords: active transport; futile cycle; integral feedback; metabolic coordination; microfluidics

Introduction

Microorganisms must acquire nutrients from the external environment. It is critical for their proliferation to take in these nutrients rapidly across cell membranes and maintain sufficient nutrient levels in the cytoplasm. Some essential nutrients are readily diffusible across the cell membrane. For example, NH_3 or CO_2 can diffuse across the membrane $\sim$30 times faster than water (Simon and Gutknecht, 1980; Walter and Gutknecht, 1986). The large membrane permeability of these molecules is both a blessing and a curse. When the ambient nutrient level is high, passive diffusion alone can supply enough nutrient needed for rapid cell growth. When the ambient level is low, however, maintaining high internal levels by active transport is challenging and costly because the transported molecules can diffuse out rapidly, resulting in a futile cycle. Thus, transporting these molecules has a steep price. However, it is not known what strategies the organisms adopt to deal with this problem.

Here, we study the management of ammonium (NH_4^+/NH_3) sequestration by *E. coli* as a model system. Nitrogen is essential for cell growth, and ammonium is the preferred nitrogen source for many microorganisms including *E. coli* (Reitzer, 2003). These microorganisms often live in environments with limited ammonium supplies, for example, μM range in fresh and seawater (Rees *et al*, 2006). Under such conditions, it is critical for their growth and survival to transport ammonium efficiently while minimizing the obligatory futile cycle.

To study how these cells manage ammonium sequestration in such ammonium-limited conditions, it is desirable to maintain low steady ammonium concentrations in the growth medium through multiple rounds of cell doubling, a very challenging task in both batch and continuous cultures (Atkinson *et al*, 2002; Soupene *et al*, 2002). Instead, we cultured cells in microfluidic chambers that can maintain nutrients including ammonium to the desired concentrations (Groisman *et al*, 2005). By monitoring the growth and gene expression of exponentially growing cells using time-lapse microscopy, and analyzing the data quantitatively using flux analysis, we reveal a delicate control of ammonium sequestration strategy: as the ambient ammonium concentration is reduced, *E. coli* cells first increase their ability to assimilate ammonium that diffuses freely across the membrane. Upon maximizing ammonium assimilation, ammonium transport by the transporter AmtB is activated abruptly, but only to the minimal level needed to sustain cell growth. The onset

of transport changes under different growth conditions that support different growth rates (and hence different cellular demands for nitrogen) when ammonium is replete, but it always occurs just at the concentration where an isogenic strain unable to transport ammonium begins to show a growth defect. Mathematical modeling of known interactions reveals an integral feedback strategy by which two distinct signals of the cellular nitrogen status are used to provide seamless coordination between ammonium assimilation and transport, such that the degree of ammonium transport is the minimum necessary to sustain cell growth.

Results

AmtB is necessary to maintain rapid cell growth at low ambient ammonium concentrations

Ammonium exists predominantly in the ionic form (NH_4^+) at neutral pH, and the minor gaseous species (NH_3) can diffuse rapidly through the cell membrane (Walter and Gutknecht, 1986). At high ambient ammonium concentrations, the passive diffusion of NH_3 can provide enough nitrogen for optimal cell growth (blue arrow, Figure 1A; Soupene *et al*, 1998; Andrade and Einsle, 2007; Fong *et al*, 2007). As the ambient ammonium concentration is reduced and active ammonium transport is needed to sustain cell growth, a wide range of organisms expresses the Amt family proteins (Boussiba *et al*, 1984; Loque and von Wiren, 2004; Andrade and Einsle, 2007) which concentrate ammonium inside cells (green arrow, Figure 1B) (Boussiba *et al*, 1984; Andrade and Einsle, 2007; Fong *et al*, 2007). However, the higher internal concentration of NH_4^+ / NH_3 imposes a dangerous futile cycle on the organism (Kleiner, 1985), as NH_3 unavoidably diffuses outward down the gradient (blue arrow), forcing a much larger ammonium uptake than the nitrogen flux needed for biosynthesis (red arrow).

To study how *E. coli* cells control its Amt protein, AmtB, at low ammonium concentrations, we developed microfluidic chambers (Groisman *et al*, 2005) which can maintain ammonium at low concentrations (Supplementary Figure 1A). Fresh medium flows actively through the channel (in green) and diffuses into the growth chambers (in red). The rapid diffusive medium exchange between the growth chambers and the surrounding channels (Supplementary Figure 1B) due to the small geometry ensures that steady low nutrient levels are maintained inside the chamber (Supplementary Note 1). This allows us to monitor the exponential growth cell growth at as low as $\sim$4 μM NH_4^+ (Supplementary Figure 1C).

To examine when AmtB becomes necessary for cell growth, we compared the exponential growth of the wild-type and Δ*amtB* strains (see Supplementary Tables 1 and 2 for strain details) in minimal medium with various NH_4^+ concentrations and saturating amounts of glycerol as the sole carbon source; the effect of different carbon sources will be discussed below. Typical phase-contrast images of cells growing in microfluidic chambers in Figure 1C show Δ*amtB* strains growing more slowly than the wild type at 12 μM of NH_4^+. With similar time-lapse images of 20–30 colonies recorded twice per doubling, we quantified the growth rate for wild-type and Δ*amtB* strains in Figure 1E; see Materials and methods. While the wild-type strain (solid black circles) maintained its growth rate from 10 mM down to a few μM, the Δ*amtB* strain (open black circles) grew more slowly below $\sim$20 μM (black arrow). Thus, AmtB is needed to sustain the growth below $\sim$20 μM NH_4^+ (gray zone).

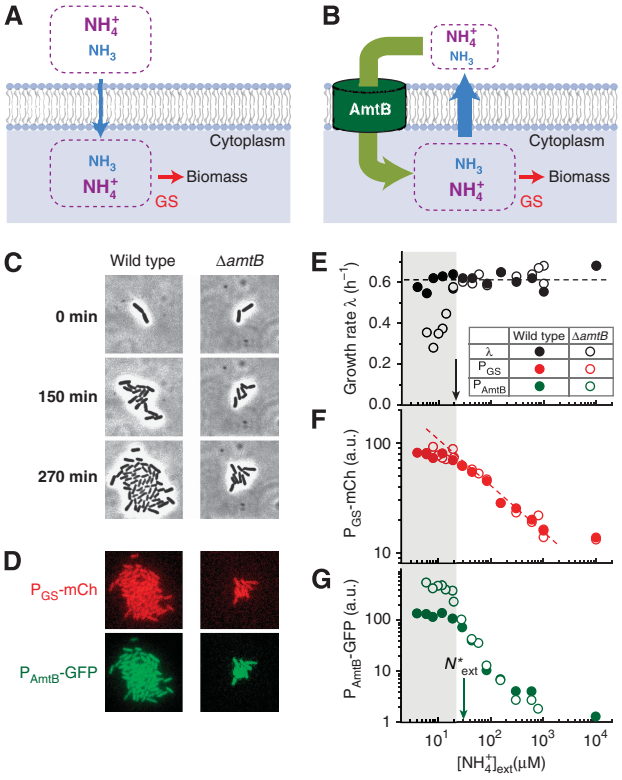

Figure 1 Ammonium sequestration by AmtB. (**A**) NH_3 is in equilibrium with NH_4^+ and diffuses across the cell membrane rapidly (blue arrow) (Walter and Gutknecht, 1986). The passive diffusion of NH_3 alone can support rapid cell growth when the ambient ammonium concentration is high (Soupene *et al*, 1998; Andrade and Einsle, 2007; Fong *et al*, 2007). Intracellular ammonium is assimilated into biomass through glutamine synthetase (GS) (Reitzer, 2003). (**B**) When the ambient ammonium concentration is low, AmtB concentrates it internally (green arrow) (Boussiba *et al*, 1984; Andrade and Einsle, 2007; Fong *et al*, 2007). Higher internal concentrations of NH_4^+ and NH_3 lead to the outward diffusion of NH_3 (blue arrow), forming an energetically costly futile cycle; see Supplementary Figure 5 for the estimate of the energetic cost. (**C**) Time-lapse phase-contrast images of *E. coli* cells growing in microfluidic chambers with minimal medium containing a very low concentration (12 μM) of NH_4Cl as the sole nitrogen source and saturating amounts of glycerol as the sole carbon source. The Δ*amtB* strain (EQ130, right) grew more slowly than the control (EQ66, left); see Supplementary Table 1 for strain details. From these images, growth rates were determined during the first three generations when the increase is clearly exponential (Supplementary Figure 1C). Here and elsewhere, the reported external NH_4^+ concentration includes a residual concentration of $\sim$4 μM estimated in the medium (Supplementary Figure 6). (**D**) mCherry (red) and GFP (green) intensities reflect the GS and *amtB* promoter activities, respectively. (**E**) While the wild type (solid circles) maintained its growth rate, the Δ*amtB* strain (open circles) grew more slowly (gray zone) below $\sim$20 μM of external NH_4^+ (black arrow), in agreement with previous findings obtained in low pH medium (Soupene *et al*, 1998, 2002; Fong *et al*, 2007); see also Supplementary Figure 7. (**F**, **G**) The promoter activities of GS (reported by mCherry, red) and AmtB (reported by GFP, green) for the wild-type (solid circle) and Δ*amtB* strain (open circle) increase as the ambient ammonium concentration is reduced. Below a characteristic NH_4^+ concentration, $N^*_{ext} \approx 30$ μM (green arrow), the GFP intensities of the two strains deviate, indicating differences in the internal nitrogen status; see text. All the data plotted here are provided in Supplementary Tables 6 and 7. a.u., arbitrary units.

GS and AmtB expression is upregulated at low ammonium concentrations

Glutamine synthetase (GS) is the major enzyme assimilating ammonium needed for cell growth at low ammonium concentrations (below 1 mM of NH_4^+) (Reitzer, 2003). K_m of GS is reported to be $\sim$100 μM for NH_4^+ (Meek and Villafranca, 1980; Alibhai and Villafranca, 1994) under physiological conditions (Supplementary Note 2). To check how the Δ*amtB* strain maintains the growth down to 20 μM NH_4^+ which is far below the K_m of GS, we monitored the expression level of GS using the mCherry fluorescence protein (Figure 1D and F). As the ambient NH_4^+ concentration was reduced, the mCherry fluorescence levels for Δ*amtB* strain (open red circles) increased gradually, beginning to approach its maximum induction level at $\sim$20 μM (right of the gray zone). GS expression of wild type (solid red circles) behaves indistinguishably. Thus, from 100 μM down to $\sim$20 μM of external NH_4^+, cell growth is maintained by elevating the GS expression level for both the wild-type and Δ*amtB* strain.

We also monitored the activity of the *amtB* promoter using a green fluorescence protein (GFP) reporter (Figure 1D). Figure 1G shows that the GFP signals of the wild-type and Δ*amtB* strain (solid and open green circles) are indistinguishable down to a characteristic ambient NH_4^+ concentration of $N^*_{ext} \approx 30$ μM (green arrow). Below this point, the GFP signal of the wild type reached a plateau while that of the Δ*amtB* strain continued to rise before leveling off at a higher plateau. Notably, the fold change of AmtB expression (>100-fold) between high ammonium ($\sim$mM of external NH_4^+) and low ammonium ($\sim$μM of external NH_4^+) conditions is much higher than that of GS expression (<10-fold in Figure 1F). Similar fold changes of AmtB and GS expression levels were observed in a bulk experiment when cells initially growing in an ammonium-replete condition transitioned to ammonium starvation (Atkinson *et al*, 2002).

Deducing the internal ammonium concentration of Δ*amtB* strain

The expression and activity levels of GS and AmtB respond to the internal nitrogen status (Reitzer, 2003). To elucidate the regulation of ammonium assimilation and transport, it is crucial to quantify the internal nitrogen status. However, there is no known way to measure directly the internal ammonium concentration *in vivo*. Here, we describe an approach to deduce it from the data in Figure 1G. We will first describe it here for the Δ*amtB* strain, which is quite straightforward. This approach will be extended below to deduce the internal ammonium concentration of wild-type cells.

The only way for the Δ*amtB* strain to acquire ammonium is through the passive diffusion of the gaseous form NH_3 (Walter and Gutknecht, 1986), with the diffusive flux $J_{diffusion}$ given by the NH_3 concentration difference between the outside and inside of cells. The latter can be related to the external and internal NH_4^+ concentrations ($[NH_4^+]_{ext}$ and $[NH_4^+]_{int}$, respectively) from the NH_4^+/NH_3 equilibrium, expressed as

$$J_{diffusion} = \kappa_{ext}[NH_4^+]_{ext} - \kappa_{int}[NH_4^+]_{int} \quad (1)$$

where κ_{ext} and κ_{int} are proportionality constants given by the NH_3 permeability, cell geometry, and extra- and intra-cellular pH; see Supplementary Equations S1–S4 for details of this derivation, and Supplementary Equations S5–S7 for the details of the proportionality constants. The definitions and values of the parameters in the constants are given in Supplementary Table 3.

For a given external NH_4^+ concentration, we can deduce the internal NH_4^+ concentration by equating the diffusion flux $J_{diffusion}$ with the rate of nitrogen assimilation, $J_{biomass}$, which is given as required by the nitrogen content of biomass (n_0) and the measured growth rate (λ), that is,

$$J_{biomass} = \lambda \times n_0. \quad (2)$$

The internal NH_4^+ concentrations ($[NH_4^+]_{int}$) of Δ*amtB* cells, deduced from Equations (1) and (2) with $J_{diffusion} = J_{biomass}$ using the measured growth rate $\lambda_{\Delta amtB}$ for each external NH_4^+ concentration (open circles in Figure 1E), are plotted for various external NH_4^+ concentrations as shown in Figure 2A (open purple circles); see Supplementary Equations S8–S11. The linear relation is expected due to the passive diffusion of NH_3 in Δ*amtB* cells. Here and below, the gray region, adopted from that in Figure 1E, indicates the conditions in which the Δ*amtB* strain exhibits reduced growth.

Deducing the GS activity

The scattered plot of P_{GS}-mCherry reporter levels observed (open circles in Figure 1F) with the deduced internal NH_4^+ concentrations for the corresponding external NH_4^+ concentrations (open circles in Figure 2A) is shown as red circles in Figure 2B, revealing a simple dependence of GS promoter activity on the internal NH_4^+ concentration. It shows that as the internal NH_4^+ concentration is reduced, the Δ*amtB* strain increases the capacity of ammonium assimilation by increasing the GS expression level. However, GS expression does not reflect the actual capacity of ammonium assimilation by GS, because GS activity can be altered by glutamine via adenylylation (Kingdon *et al*, 1967; Wulff *et al*, 1967; Okano *et al*, 2010) and by the end products of glutamine metabolism via allosteric inhibition (Woolfolk and Stadtman, 1964; Woolfolk and Stadtman, 1967). With the knowledge of the internal NH_4^+ concentrations (open circles in Figure 2A), we can further deduce GS activity from the growth rate and GS expression (open circles in Figure 1E and F) as described below.

First, the total flux of ammonium assimilation by GS per cell volume, J_{GS}, is given by the Michaelis–Menten kinetics (Meek and Villafranca, 1980),

$$J_{GS} = V_{GS} \times \frac{[NH_4^+]_{int}}{[NH_4^+]_{int} + K_{GS}} \quad (3)$$

Here, V_{GS} and K_{GS} are the associated V_{max} and the Michaelis constant, with $K_{GS} \sim 100$ μM for NH_4^+ (Meek and Villafranca, 1980; Alibhai and Villafranca, 1994). Molecularly, V_{GS} is determined by the levels of GS expression and its specific activity, with the latter affected by allosteric product inhibition (Woolfolk and Stadtman, 1964; Woolfolk and Stadtman, 1967) and reversible adenylylation (Kingdon *et al*, 1967; Wulff *et al*, 1967; Okano *et al*, 2010).

Since GS is the key enzyme assimilating internal ammonium into biomass at low ambient NH_4^+ concentrations (e.g., <1 mM; Reitzer, 2003), the ammonium assimilation flux J_{GS}

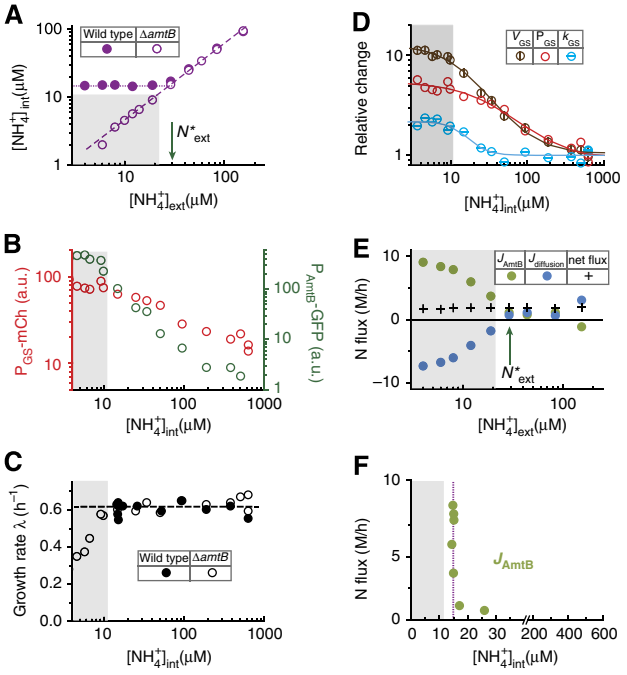

Figure 2 Steady maintenance of internal ammonium and the abrupt activation of AmtB. (**A**) The deduced internal NH_4^+ concentrations of the Δ*amtB* strain (EQ130, open purple circles) and wild type (EQ66, solid purple circles) grown in glycerol with varying NH_4^+ concentrations; see Equations (1) and (2), and the text. The gray region (defined in Figure 1E) indicates the conditions in which the Δ*amtB* strain exhibits reduced growth. (**B**) The dependences of the GS (left axis) and *amtB* (right axis) promoter activities of the Δ*amtB* strain on the deduced internal NH_4^+ concentrations. (**C**) The growth rate of the Δ*amtB* strain and wild type on the deduced internal NH_4^+ concentrations. (**D**) The V_{max} of GS (V_{GS}, brown), the GS expression level (P_{GS}, red) and the specific activity of GS (k_{GS}, cyan) are plotted relative to their values in ammonium-replete conditions. Here, V_{GS} is obtained from Equation (3), and k_{GS} is obtained from the ratio of V_{GS} and P_{GS}. The lines of respective colors are fit using Hill functions (Supplementary Equation S18); see Supplementary Table 4 for the kinetic parameters of the fit. (**E**) The deduced ammonium transport flux through AmtB (green circles) and the NH_3 diffusion flux (blue circles); see Equations (1), (2) and (4). Black crosses represent the net nitrogen influx (the sum of the two fluxes), which the cells utilize for biomass synthesis. Note that the maintenance of the net flux is accompanied by strong increases in ammonium transport by AmtB, and NH_3 leakage through passive diffusion. (**F**) A sharp increase in the ammonium transport flux through AmtB (green circles) when plotted against the deduced internal NH_4^+ concentrations.

can be obtained from the nitrogen demand for cellular growth, $J_{biomass} = \lambda_{\Delta amtB}\, n_0$ (Equation (2)), where $\lambda_{\Delta amtB}([NH_4^+]_{int})$, shown as the open circles in Figure 2C, is obtained from the measured growth rates in various external NH_4^+ concentrations (open circles in Figure 1E) and the corresponding internal NH_4^+ concentrations (open circles in Figure 2A). Using this resulting form of $J_{GS}([NH_4^+]_{int})$ in Equation (3) yields V_{GS} for various internal NH_4^+ concentrations, plotted as brown circles with vertical lines in Figure 2D. In the same figure, the relative GS expression level, $P_{GS}([NH_4^+]_{int})$, from Figure 2B (red circles) is re-plotted as red circles for comparison. The ratio of $V_{GS}([NH_4^+]_{int})$ and $P_{GS}([NH_4^+]_{int})$ gives the relative changes in the specific activity of GS, k_{GS}, at the different internal NH_4^+ concentrations, shown as the cyan circles with horizontal lines in Figure 2D. As the internal NH_4^+ concentration is reduced, $k_{GS}([NH_4^+]_{int})$ increases by ~2-folds, approaching its maximum level near the concentration at which $P_{GS}([NH_4^+]_{int})$ is maximized. Previously, it was found from batch culture studies that GS is approximately half-adenylylated in nitrogen-replete conditions and completely unadenylylated in nitrogen-limited conditions (Okano *et al*, 2010). Thus, the changes in k_{GS} may arise primarily from the changes in the adenylylation state. We note that V_{GS}, P_{GS} and k_{GS} can be well described by Hill functions (Supplementary Equation S18), as shown by the lines of respective colors in Figure 2D: see Supplementary Table 4 for parameters of the fit.

Deducing the AmtB activity

In contrast to the Δ*amtB* strain that relies only on passive diffusion of NH_3 for ammonium uptake, wild-type cells can employ AmtB to actively transport ammonium. However, a futile cycle associated with the ammonium transport (Figure 1B) may impose a significant burden on cells. Thus, it is critical for cells to control the AmtB activity tightly. This can be seen from the comparison of the *amtB* promoter activities between wild-type and Δ*amtB* strains (Figure 1G); they are indistinguishable down to the low external NH_4^+ concentration marked with N^*_{ext} below which they deviate, indicating that the internal nitrogen status of the two strains differs below N^*_{ext}. This suggests that although AmtB expression is upregulated below ~1 mM of external NH_4^+, its activity is turned on only below N^*_{ext}, which is slightly above when is needed to maintain rapid growth (gray region). Indeed, it is known the AmtB activity is inhibited by the regulatory protein GlnK, which is expressed in the same operon as AmtB, binds tightly to it, and inhibits its activity in ammonium-replete conditions (Coutts *et al*, 2002; Blauwkamp and Ninfa, 2003; Javelle *et al*, 2004).

We wish to determine AmtB activity quantitatively. Since this information is contained in the internal NH_4^+ concentration which is directly affected by AmtB activity, we determine the internal NH_4^+ concentration of wild type first and extract the AmtB activity from it. To deduce the internal NH_4^+ concentration of the wild type, we make a scattered plot (green circles in Figure 2B) of P_{AmtB}-GFP reporter levels measured for the Δ*amtB* strain at various external NH_4^+ concentrations (open circles in Figure 1G) against the corresponding internal NH_4^+ concentrations (open circles in Figure 2A), which reveals a simple and sensitive dependence of the *amtB* promoter activity on the internal NH_4^+ concentration. Assuming that the dependence is the same for the wild-type cells, which amounts to the assumption that the *amtB* promoter activity is primarily determined by the internal NH_4^+ concentration only when the ambient NH_4^+ concentration is varied (Supplementary Note 3), the internal NH_4^+ concentration of the wild type can be directly read off from the measured *amtB* promoter activity in wild-type cells (solid circle in Figure 1G). The internal NH_4^+ concentration obtained in this way is shown as the solid purple circles in Figure 2A. It is seen to be *maintained* at ~15 μM as the external NH_4^+ concentration is reduced below $N^*_{ext} \approx 30$ μM (green arrow in Figure 2A).

With the knowledge of the internal NH_4^+ concentration of the wild-type cells, we can deduce the total activity of AmtB, J_{AmtB}, defined as the ammonium transport flux through AmtB

(Supplementary Equation S13), by balancing the supply and assimilation of nitrogen: for exponentially growing wild-type cells, the active ammonium transport by AmtB must supply for both the nitrogen needed for growth and the passive out diffusion of NH_3 through the membrane (Figure 1B). Thus, we have

$$J_{\mathrm{AmtB}} + J_{\mathrm{diffusion}} = J_{\mathrm{biomass}}, \quad (4)$$

where $J_{\mathrm{diffusion}}$ and J_{biomass} are given by Equations (1) and (2), respectively: see Supplementary Equations S12–S15 for details. The external and internal NH_4^+ concentrations of the wild-type cells given in Figure 2A (solid circles) yield the diffusion flux $J_{\mathrm{diffusion}}$, plotted against the external NH_4^+ concentration as the blue circles in Figure 2E, with the negative values indicating a flux out of the cell (see also the blue arrow in Figure 1B). Together with J_{biomass} from the observed growth rate of wild-type cells (solid circles in Figure 1E), J_{AmtB} is deduced from Equation (4); the results are plotted as the green circles in Figure 2E. Note that this analysis does not depend on the exact molecular species (NH_4^+ versus NH_3) transported by AmtB, a contentious subject in the literature (Andrade and Einsle, 2007; Fong *et al*, 2007). The ammonium transport flux through AmtB here only refers to the rate of nitrogen atoms being transported. In Figure 2E, we also indicate the net ammonium uptake flux, given by the sum of $J_{\mathrm{diffusion}}$ and J_{AmtB}, as the crosses. It is clear that net uptake flux is much ($\sim$5-fold) smaller than the flux through AmtB in the gray region where AmtB activity is needed, indicating that much of the flux through AmtB is lost back to the medium by diffusion as will be discussed below.

The activity of AmtB is delicately controlled

The internal NH_4^+ concentrations and AmtB activity deduced above reveal a delicate management of ammonium sequestration by wild-type cells. In Figure 2A, the internal NH_4^+ concentrations for wild-type and Δ*amtB* strain are indistinguishable for ambient NH_4^+ concentrations above $N^*_{\mathrm{ext}} \approx 30\,\mu M$ (green arrow), both decreasing linearly. Below that point, however, the internal NH_4^+ concentrations of Δ*amtB* strain continued to decrease linearly whereas the wild type maintained its internal NH_4^+ concentration at an approximately constant value ($\sim 15\,\mu M$), referred to as the 'maintenance concentration' (purple dotted line). The deviation of internal NH_4^+ concentrations for the two strains below $N^*_{\mathrm{ext}} \approx 30\,\mu M$ (green arrow) is accompanied by a strong increase in ammonium transport by AmtB (J_{AmtB}, green circles in Figure 2E), and in NH_3 back diffusion ($J_{\mathrm{diffusion}}$, blue circles). Importantly, the net ammonium influx (black crosses) remained unchanged, providing a steady flow of nitrogen needed for biomass synthesis at the constant growth rate. The dependence of the ammonium transport on the availability of internal ammonium (Figure 2F) shows that the ammonium flux through AmtB increased sharply at the maintenance concentration (purple dotted lines in Figure 2A and F), which is slightly above the concentration at which the Δ*amtB* strain begins to grow slowly (gray zone in Figure 2C and F).

These observations highlight the sensitive and precise control of AmtB activity, which is crucial in light of the futile cycle associated with it. The ammonium transport by AmtB enables cells to maintain their optimal growth at low ambient NH_4^+ concentrations (solid circles in gray region in Figure 1E) by concentrating NH_4^+ internally (below N^*_{ext} in Figure 2A). However, the higher internal NH_4^+ concentrations result in large leaky flux of NH_3 (blue circles in Figure 2E and blue arrow in Figure 1B), forcing cells to transport more ammonium than necessary (green circles in Figure 2E and green arrow in Figure 1B). To minimize the futile cycle, cells exert a tight control on AmtB activity. As the ambient ammonium concentration is reduced, they first increase the ability to assimilate NH_3 diffusing into the cytoplasm by increasing GS expression/activity (Figures 1F and 2D), but keep AmtB inactive (green circles above N^*_{ext} in Figure 2E). Only as GS expression/activity approaches the maximum (the gray zone in Figures 1F and 2D, also the region where the lack of AmtB would slow down growth as in Figures 1E and 2C), AmtB is activated abruptly (Figure 2F) and transports just enough ammonium to maintain the internal NH_4^+ barely above the minimum level needed for optimal growth (purple dotted line above gray zone in Figure 2A and F), thereby minimizing the futile cycle.

The delicate control of AmtB activity is coordinated with cellular nitrogen demand

Cells coordinate nitrogen and carbon metabolism through various mechanisms (Commichau *et al*, 2006; Doucette *et al*, 2011). Since cells growing on different carbon sources exhibit different growth rates in ammonium-replete conditions and hence have different demands for nitrogen, we varied the carbon source in the growth medium to ones that provided successively faster growth than what glycerol can provide. We expect this would force the cells to activate AmtB at higher ammonium concentrations if the faster growth rates are to be maintained as the external ammonium concentration is reduced. Indeed, the data on growth rates (Figure 3A) show that the wild type (solid symbols) was able to maintain growth throughout the range of NH_4^+ concentrations tested. In contrast, the Δ*amtB* strain (open symbols) exhibited growth reduction as the ambient NH_4^+ concentration was reduced, and the onset of the growth defect (black arrows) occurred at *successively higher* ambient NH_4^+ concentrations for the medium supporting faster growth. Also, Figure 3B shows that the NH_4^+ concentrations at which the *amtB* promoter activity (GFP) of the wild-type and Δ*amtB* strain deviate (green arrows) are always just slightly above the respective onset of the growth defect for the three carbon sources tested.

The internal NH_4^+ concentration and the NH_4^+ flux through AmtB were subsequently deduced from the data in Figure 3A and B as described above, for wild-type cells grown in the two additional types of medium. The internal NH_4^+ concentrations were again maintained at constant values at low ambient NH_4^+ concentrations (solid purple symbols in Figure 3C), with successively higher maintenance concentrations for the faster growing cells, consistent with the higher internal NH_4^+ concentrations needed for assimilation by GS at the higher rates. The growth rate and the ammonium flux through AmtB are plotted against the internal NH_4^+ concentrations for the three medium studied in Figure 3D (black and green symbols,

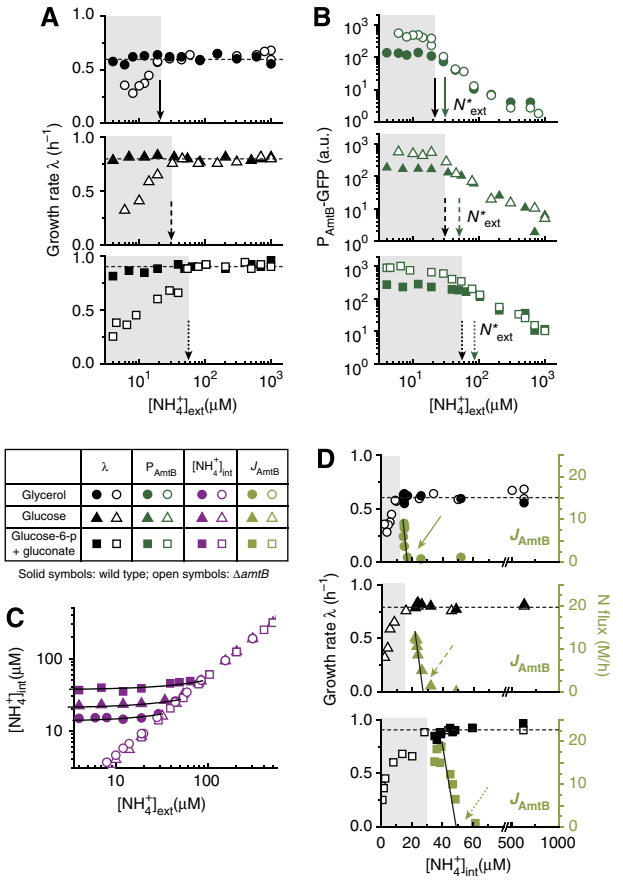

Figure 3 Coordination of AmtB activity with the cell's growth status. The growth rate of the culture in ammonium-replete condition was changed by using different carbon sources: glucose-6-phosphate (g6p) plus gluconate (squares), and glucose (triangles). Data from Figures 1 and 2 (glycerol as the carbon source) are re-plotted for comparison (circles). Solid, dashed, and dotted arrows are associated with glycerol, glucose, and g6p plus gluconate. Solid and open symbols indicate the wild-type and Δ*amtB* strain (EQ66 and EQ130), respectively. (**A**) The growth rate of the wild-type and Δ*amtB* strain for all carbon sources tested. The onset of the growth defect of the Δ*amtB* strain (black arrows) was at successively higher ambient NH_4^+ concentrations for the carbon sources supporting faster growth. (**B**) The *amtB* promoter activities (reported by GFP) of the wild-type and Δ*amtB* strains deviated (green arrows) at slightly higher ambient NH_4^+ concentrations than where growth defect set in for the Δ*amtB* strain (gray zone), indicating that ammonium transport in the wild type occurred barely above where it would be needed to maintain the growth, in coordination with the different growth conditions. (**C**) The maintenance of the internal NH_4^+ concentration for the different carbon sources. (**D**) The growth rate (black symbols) and ammonium transport flux (green symbols) plotted against the internal NH_4^+ concentrations for the different carbon sources. The abrupt increase in the ammonium flux occurred above the respective onset of growth defect of the Δ*amtB* strain (right of the gray zone). The black lines in Figures 3C and D show the linear fits of our model (Supplementary Equations S36–S38), from which the onset of AmtB activation N_{int}^* is determined (green arrows); see Supplementary Table 5 for the parameters. All the data plotted here are given in Supplementary Tables 8–11. a.u., arbitrary units.

respectively). We see that for each medium studied, the abrupt increase in ammonium flux occurred at a value of N_{int}^* (green arrows in Figure 3D) which is slightly above the respective onset of growth defect of the Δ*amtB* strain (the right of gray region); see Supplementary Table 5 for the values of N_{ext}^*, N_{int}^* and the onset of growth defect of the Δ*amtB* strain. These results show that the onset of ammonium transport and the maintenance level of the internal NH_4^+ is not preset to a fixed value, but is instead determined dynamically, such that ammonium transport by AmtB is only employed as necessary to maintain cell growth.

Discussion

Glutamine is unlikely to be a signal controlling AmtB activity

The delicate control of AmtB activity and its coordination with cellular nitrogen demand require intricate signaling system(s). Glutamine has long been established as a signal of the internal nitrogen status (Reitzer, 2003), serving as the major effector of GS expression (Hirschman *et al*, 1985; Reitzer and Magasanik, 1986; Jiang *et al*, 1998a, b) and activity (Kingdon *et al*, 1967; Wulff *et al*, 1967; Okano *et al*, 2010) (Figure 4A). It is therefore a possible candidate for controlling AmtB activity, via for example, the known effect of glutamine on GlnK that inhibits AmtB (Coutts *et al*, 2002; Javelle *et al*, 2004). The intracellular glutamine concentration unfortunately cannot be directly measured for cells grown under the very low ammonium conditions provided by the microfluidic chambers, due to the small number of cells in the chambers. However, because GS is the sole assimilator of ammonium at low ambient NH_4^+ concentrations (Reitzer, 2003), the negative feedback regulation of glutamine on GS imposes an obligatory relation between the internal NH_4^+ concentration and the glutamine pool which can be deduced from two relations: (i) the empirically obtained relation between the relative P_{GS}-mCherry promoter activity and the internal NH_4^+ concentration, $P_{GS}([NH_4^+]_{int})$ (red circles and line in Figure 2D) and (ii) the mechanism regulating GS expression, controlled primarily by the glutamine concentration [Gln] under nitrogen limitation (Hirschman *et al*, 1985; Reitzer and Magasanik, 1986; Jiang *et al*, 1998a, b; Reitzer, 2003).

Writing the relative GS expression as $E_{GS}([Gln])$, the relation between [Gln] and $[NH_4^+]_{int}$ follows readily by equating $P_{GS}([NH_4^+]_{int})$ and $E_{GS}([Gln])$. We model $E_{GS}([Gln])$ by a Hill function with the Michaelis parameter K_e^{Gln}, maximum fold-change f_e^{Gln}, and a Hill coefficient H_e^{Gln} (see Supplementary Equation S19), whose values are highly constrained by existing data on GS expression and glutamine concentration (Ikeda *et al*, 1996; Atkinson *et al*, 2002; Okano *et al*, 2010); as shown in Supplementary Figure 2, the existing data are best described by $K_e^{Gln} \approx 1.5$ mM, $f_e^{Gln} \approx 5$ and $H_e^{Gln} \geqslant 6$. Comparing $E_{GS}([Gln])$ with the Hill function for $P_{GS}([NH_4^+]_{int})$ described by the red line in Figure 2D, we obtain

$$[Gln] \propto ([NH_4^+]_{int})^{0.2} \quad (5)$$

which is plotted in Figure 4B (see Supplementary Equations S18–S20 for details). It shows an extremely weak dependence of the glutamine pool on the internal NH_4^+ concentration, reflecting the homeostatic nature of negative feedback control by glutamine (Reitzer, 2003).

The weak dependence of the glutamine pool on the internal NH_4^+ concentration, together with the steady maintenance of the internal NH_4^+ concentration when AmtB activity abruptly increases (Figure 2F), makes it unlikely for glutamine to be the

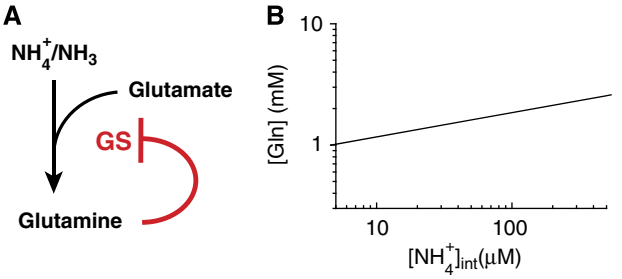

Figure 4 GS regulation by glutamine and the relation between glutamine pool and internal ammonium concentration. (**A**) At low ambient ammonium concentrations, GS is the major ammonium assimilation enzyme, catalyzing the formation of glutamine from ammonium and glutamate (Reitzer, 2003). GS expression is repressed by glutamine (red line) through the NtrBC two-component signaling system (Hirschman *et al*, 1985; Reitzer and Magasanik, 1986; Jiang *et al*, 1998a, b) while the specific activity of GS is inhibited by adenylylation by GlnE whose activity is stimulated by glutamine (Kingdon *et al*, 1967; Wulff *et al*, 1967; Okano *et al*, 2010). (**B**) This negative feedback regulation of glutamine on GS imposes an obligatory relation between the internal NH_4^+ concentration and the glutamine pool, described by Equation (5): see text and Supplementary Equations S18–S20 for details. As shown in the plot, this obligatory relation features a very weak dependence of the glutamine pool on the internal NH_4^+ concentration, reflecting the homeostatic nature of negative feedback control by glutamine (Reitzer, 2003).

major effector of AmtB activity. This is further supported by the results of Figure 3D, which show that AmtB transport is activated at *different* internal NH_4^+ concentrations (and hence different glutamine concentrations) under the different growth conditions.

AmtB is regulated by α-ketoglutarate via an integral feedback control

The known molecular interactions actually suggest an alternative signaling scheme as depicted in Figure 5A. It is known that GlnK binds tightly to AmtB and inhibits its activity in ammonium-replete conditions (brown dashed line) (Coutts *et al*, 2002; Blauwkamp and Ninfa, 2003; Javelle *et al*, 2004). Also, GlnK dissociates from AmtB at elevated α-ketoglutarate (aKG) concentrations, as predicted by Gruswitz *et al* (2007) and later confirmed by Radchenko *et al* (2010) and Truan *et al* (2010), thereby setting AmtB free to transport ammonium (cyan dashed line). What ties these two pieces of biochemical interactions together is that the aKG pool can be dramatically affected by the ammonium influx which it controls, as established in the literature (Yuan *et al*, 2009; Radchenko *et al*, 2010; Doucette *et al*, 2011; Yan *et al*, 2011). At low internal ammonium concentrations, ammonium is assimilated by the GS/GOGAT cycle (Supplementary Figure 3; Reitzer, 2003), producing glutamate (Glu) from aKG (red arrows in Figure 5A). The nitrogen group in Glu is passed on to various precursors for biomass synthesis, turning Glu back to aKG (black arrows). If the internal ammonium level drops, then the rate of ammonium assimilation will drop immediately. This slows aKG drainage (red arrow), resulting in aKG accumulation: see Supplementary Figure 3 for details. Indeed, the rapid accumulation of aKG upon ammonium downshift (>5-folds within 15 s) was reported recently (Yan *et al*, 2011).

Quantitative description of these processes elucidates an intriguing integral feedback scheme. Integral feedback is an effective control scheme to stabilize a complex system to a desired set point (Leigh, 2004). Importantly, when the system deviates from the desired set point, a control variable integrates the deviation and activates a controller to reduce it, maintaining the system at the desired set point robustly. In the regulation of ammonium transport, aKG and AmtB serve as the control variable and controller, respectively. The aKG pool ([aKG]) is balanced primarily by the rate of nitrogen incorporation into biomass (J_{biomass}, black arrow in Figure 5A), and ammonium assimilation rate (J_{GS}, red arrow), that is,

$$\frac{\mathrm{d}}{\mathrm{dt}}[\mathrm{aKG}] = J_{\mathrm{biomass}} - J_{\mathrm{GS}}. \qquad (6)$$

J_{GS} is provided by the sum of the NH_3 influx via diffusion ($J_{\mathrm{diffusion}}$, blue arrow) and the AmtB transport flux (J_{AmtB}, green arrow), that is,

$$J_{\mathrm{GS}} = J_{\mathrm{diffusion}} + J_{\mathrm{AmtB}}([\mathrm{aKG}]) \qquad (7)$$

with J_{AmtB} being an increasing function of [aKG] (Radchenko *et al*, 2010).

In a steady state, Equations (6) and (7) yield

$$J_{\mathrm{biomass}} = J_{\mathrm{GS}} = J_{\mathrm{diffusion}} + J_{\mathrm{AmtB}}([\mathrm{aKG}]). \qquad (8)$$

As described above, $J_{\mathrm{GS}}([NH_4^+]_{\mathrm{int}})$ is obtained from $n_0 \times \lambda_{\Delta amtB}([NH_4^+]_{\mathrm{int}})$; its form is sketched in Figure 5B based on the form of $\lambda_{\Delta amtB}([NH_4^+]_{\mathrm{int}})$ in Figure 2C. Under ammonium-replete conditions, $J_{\mathrm{GS}} = \lambda \times n_0$ with the growth rate λ determined by other metabolic constraints (such as the carbon source). However, as the internal NH_4^+ concentration $[NH_4^+]_{\mathrm{int}}$ decreases, J_{GS} eventually decreases when $[NH_4^+]_{\mathrm{int}}$ decreases below a certain level, N^*_{int} (the gray zone). Thus for the cell to maintain growth at the rate λ, it is necessary to keep $[NH_4^+]_{\mathrm{int}} \geqslant N^*_{\mathrm{int}}$ (above the gray zone in Figure 5B). This can be accomplished by passive diffusion alone (i.e., $J_{\mathrm{AmtB}} = 0$) for sufficiently large external NH_4^+ concentration, $[NH_4^+]_{\mathrm{ext}}$, or by turning on the AmtB flux when the external NH_4^+ concentration is so low that $[NH_4^+]_{\mathrm{int}}$ would drop below N^*_{int} by passive diffusion alone. The latter scenario can be mediated by aKG according to Equation (6) since any decrease in J_{GS} due to $[NH_4^+]_{\mathrm{int}} < N^*_{\mathrm{int}}$ (Figure 5B) would result in aKG accumulation (control variable), which then activates AmtB (Gruswitz *et al*, 2007; Radchenko *et al*, 2010; Truan *et al*, 2010) (controller) until the steady-state condition defined by Equation (8) is restored.

The robust maintenance of internal ammonium concentration and the abrupt onset of ammonium transport through AmtB

The above mode of regulation ensures that AmtB is activated only when $[NH_4^+]_{\mathrm{int}}$ decreases below N^*_{int}. The steady-state concentrations of aKG and internal ammonium that determine the AmtB activity can be readily deduced from Equation (8) assuming a generic Hill form for the activation of J_{AmtB} by aKG. For $[NH_4^+]_{\mathrm{ext}} > N^*_{\mathrm{ext}}$, the passive diffusion alone can supply for enough nitrogen needed for cell growth and AmtB is inactive ($J_{\mathrm{AmtB}} \approx 0$). There, [aKG] remains at its basal level (cyan line in

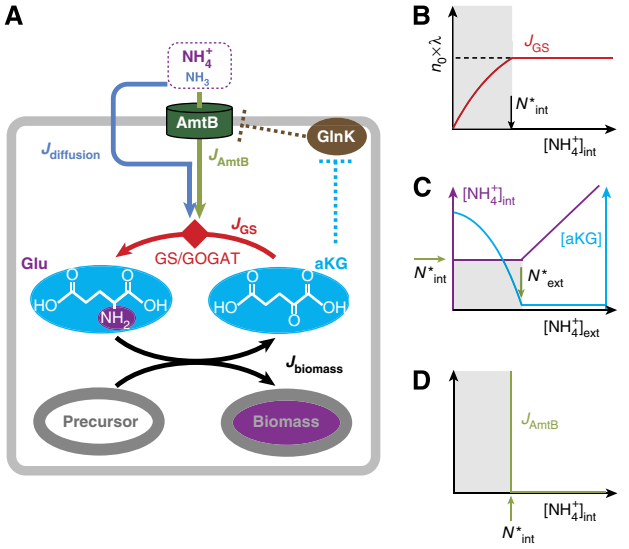

Figure 5 The integral feedback model of AmtB activation control. (**A**) Intracellular ammonium is assimilated into the biomass in two steps: first, it is captured in the form of glutamate (Glu) using the carbon skeleton α-ketoglutarate (aKG) via the GS/GOGAT pathway; see Supplementary Figure 3 for details. Then, the N-group in Glu is transferred to various carbon precursors to synthesize amino acids and incorporated into the biomass, while recycling the carbon skeleton back to aKG. Importantly, the aKG pool, which integrates imbalances between the ammonium assimilation flux (J_{GS}) and the biomass incorporation flux ($J_{biomass}$) (Equation (6)), is known to activate AmtB strongly (Gruswitz *et al*, 2007; Radchenko *et al*, 2010; Truan *et al*, 2010) via the regulatory GlnK (Coutts *et al*, 2002; Blauwkamp and Ninfa, 2003; Javelle *et al*, 2004), as indicated by the dashed cyan and brown lines. These interactions form the integral feedback loop (Equations (6)–(8)). (**B**) The flux of ammonium assimilation by GS, J_{GS}, plotted against the internal ammonium concentration, $[NH_4^+]_{int}$. J_{GS} is obtained from $\lambda \times n_0$, based on the form of $\lambda_{\Delta amtB}([NH_4^+]_{int})$ shown in Figure 2C. J_{GS} decreases when $[NH_4^+]_{int}$ decreases below a certain level, N^*_{int} (gray region). (**C**, **D**) The steady-state aKG concentration ([aKG], cyan), internal ammonium concentration (purple), and AmtB activity (J_{AmtB}, green) are deduced from Equation (8); see Supplementary Figure 4 for detailed explanation. N^*_{ext} is the external ammonium concentration ($[NH_4^+]_{ext}$) below which J_{GS} decreases without AmtB. For $[NH_4^+]_{ext} > N^*_{ext}$, [aKG] remains at its basal level, and $[NH_4^+]_{int}$ changes linearly with $[NH_4^+]_{ext}$. For $[NH_4^+]_{ext} < N^*_{ext}$, [aKG] increases and activates AmtB to the level needed to uphold $[NH_4^+]_{int}$ at N^*_{int}.

Figure 5C), and $[NH_4^+]_{int}$ changes linearly (purple line) with $[NH_4^+]_{ext}$ as described by Equation (8), together with $J_{diffusion}$ given by Equation (1). For $[NH_4^+]_{ext} < N^*_{ext}$, AmtB is activated only to uphold $[NH_4^+]_{int}$ at N^*_{int} with the activity determined by Equation (8). [aKG] is raised to the level needed, while $[NH_4^+]_{int}$ remains at N^*_{int}; see Supplementary Figure 4 for details.

The feedback scheme described here ensures that $[NH_4^+]_{int} \approx N^*_{int}$ while J_{AmtB} increases for $[NH_4^+]_{ext} < N^*_{ext}$, giving rise to three prominent features: (i) the robust maintenance of internal ammonium at the minimum level (N^*_{int} in Figure 5C) needed to sustain the growth is achieved autonomously without the need of fine-tuning parameters (the characteristics of an integral feedback control). (ii) A plot of J_{AmtB} versus $[NH_4^+]_{int}$ must inevitably have an abrupt increase of J_{AmtB} at N^*_{int} as shown in Figure 5D. Notably, neither of these features requires any cooperative molecular interactions. (iii) The abrupt activation of AmtB is not preset, but is determined by the onset of the decrease in J_{GS} (N^*_{int} in Figure 5B and D); see Equation (6). As a result, AmtB activation is adjusted automatically to maintain rapid cell growth in different ammonium-limiting conditions.

The perfect maintenance of the internal NH_4^+ concentration for $[NH_4^+]_{int} < N^*_{ext}$ (horizontal purple line in Figure 5C) and infinitely sharp activation of AmtB (vertical line in Figure 5D) in the simple feedback model described here resemble qualitatively the data shown in Figure 3C and D. However, the actual maintenance of the internal NH_4^+ is not perfect but has minor declines (Figure 3C); also the activation of AmtB is not infinitely sharp but occurs over a narrow range of $[NH_4^+]_{int}$ (Figure 3D). These modest blurring effects can be readily accounted for by the known (weak) effect of the stimulation of J_{GS} by aKG (Jiang *et al*, 1998b, c; Reitzer, 2003). Although we described that J_{GS} depends only on $[NH_4^+]_{int}$ with a well-defined N^*_{int} (Figure 5B) in our simple model, it is known that aKG has a marginal effect on J_{GS} via changes in GS expression and specific activity (Jiang *et al*, 1998b, c; Reitzer, 2003). Thus, when the aKG concentration increases for $[NH_4^+]_{ext} < N^*_{ext}$ (cyan curve in Figure 5C), the resulting weak increase in J_{GS} allows minor declines in $[NH_4^+]_{int}$ below N^*_{int} without slowing down growth. We included this effect in the more elaborate analysis described in Supplementary information (Supplementary Equations S24–S39). The extended model adequately explains the data in Figure 3C and D (black lines). It showed that the slopes of the minor decline in the maintenance of internal NH_4^+ and in the activation of AmtB (Figure 3C and D) were determined by one parameter, reflecting the response of GS expression and activity relative to that of AmtB activity as aKG concentration changes.

Tight coordination of GS and AmtB activities

For $[NH_4^+]_{ext} > N^*_{ext}$, $[NH_4^+]_{int}$ (purple curve in Figure 5C) changes with $[NH_4^+]_{ext}$ while [aKG] (cyan curve) remains constant. For $[NH_4^+]_{ext} < N^*_{ext}$, [aKG] changes while $[NH_4^+]_{int}$ remains constant. The interlaced dependence of $[NH_4^+]_{int}$ and [aKG] on the external NH_4^+ concentration highlights the tight coordination of the two lines of defense against ammonium shortage. For the external NH_4^+ concentration above N^*_{ext}, glutamine (via the obligatory relation with $[NH_4^+]_{int}$ described by Equation (5)) can be an effective controller of the nitrogen status, increasing the capacity to assimilate the gaseous NH_3 diffusing into the cytoplasm by upregulating increasing GS expression and activity (Figures 1F and 2D; Reitzer, 2003). However, for the external NH_4^+ concentration below N^*_{ext}, $[NH_4^+]_{int}$ is kept frozen at its maintenance level N^*_{int} (purple line in Figure 5C). There, it is aKG which senses the nitrogen status and activates transport by AmtB (cyan line in Figure 5C and green line in Figure 5D).

Glutamine has long been established as a signal of the internal nitrogen status (Ikeda *et al*, 1996; Reitzer, 2003). aKG is a well-known signal of internal nitrogen status for other organisms, such as cyanobacteria (Muro-Pastor *et al*, 2001). Here, we established that aKG is also a signal of the internal nitrogen status at very low ammonium concentrations. The key point here is that the two distinct signaling pathways are needed to provide the seamless shift of the need-based

ammonium acquisition strategy, from the upregulation of assimilation by GS to the upregulation of transport by AmtB.

Perspective

As the ambient ammonium level is reduced, cells step up the transport of ammonium and keep growing as fast as permitted by other (e.g., carbon) conditions, in spite of clues of a possible nitrogen crisis (i.e., the depletion of ambient ammonium). Despite this seemingly lavish strategy, however, the integral feedback scheme ensures that NH_4^+ is not transported more than necessary. This tight control may be necessary in light of a very high cost of ammonium transport, estimated to be a substantial part of the cellular energy budget (see Supplementary Figure 5 for the estimate of the associated energy cost), due to the obligatory futile NH_3 cycle (Figure 1B). This result is directly applicable to microorganisms in the marine environment in which ammonium concentration is very low (Rees *et al*, 2006). Furthermore, similar strategies may underlie how organisms deal with other essential but highly permeable nutrients.

Materials and methods

Strain and media

All strains were derived from *Escherichia coli* K12 strain NCM3722 (Soupene *et al*, 2003; Lyons *et al*, 2011) as listed in Supplementary Table 1 and detailed in Supplementary Methods. MOPS-buffered minimal media (pH 7.4) were used for cell growth as described by Neidhardt *et al* (1974). For carbon sources, glycerol (0.4% w/v), glucose (0.4% w/v), or 10 mM each of glucose-6 phosphate and gluconate were used. For nitrogen sources, different concentrations of NH_4Cl were used as specified. All the media were filtered through 0.45 μm filters.

Microfluidic device fabrication

Microfluidic devices were fabricated by molding silicone elastomer (PDMS Slygard 184, Dow Corning) to the master molds (Groisman *et al*, 2005), consisted of two layers of cross-linked epoxy (Su-8s, MicroChem) patterned by negative phototransparency masks (FineLine Imaging, CO) on silicon wafers (Supplementary Figure 1A). The layer for growth chambers (~1.5 μm) was deposited first using SU-8 2002 and processed according to manufacturer's manual. On top of the first layer, the second layer for channels (~25 μm) was deposited using SU-8 2025 (side view).

PDMS was mixed 1:15 ratio of catalyst and resin, poured to the master mold, degassed for 30 min and cured in an 80°C oven for 90 min. After the elastomer was peeled off the mold, inlet and outlet holes were punched. Then, the device was boiled in 1% HCl solution for 1 h, attached to No. 1 microscope cover glass (pre-cleaned with ethanol) and baked in the 80°C oven overnight for maximum binding.

Cell growth in microfluidic chamber

All cultures were grown at 37°C. The cells were first cultured in LB broth in 20 mm test tubes with shaking (250 r.p.m.) in a water bath (New Brunkswick Scientific). After 5–6 h of growth, they were transferred to a MOPS medium containing the selected carbon source with 20 mM of NH_4Cl and grew overnight in the same condition (pre-culture). The pre-culture was inoculated with fewer than 10^5 cells/ml so that cells were in an exponential phase at the time of experiment. The next morning, the pre-culture was diluted to a fresh growth medium containing the same concentration of NH_4Cl as in the experimental growth medium, and 0.1% BSA (bovine serum albumin, Sigma; BSA prevents cells from binding to surfaces of microfluidic devices) to an optical density (OD_{600}) of 0.005–0.01 as measured on a Genesys20 spectrophotometer (Thermo-Fisher) with the standard sample holder (16.100-Q-10/Z8.5, Starna Cells Incl; ~200 μl per measurement). To load cells into the microfluidic device, the diluted pre-culture was pressured at 1–2 psi to the outlet of the device (Supplementary Figure 1A). After the channel and growth chambers were completely filled with the pre-culture, the culture was removed and a fresh experimental growth medium was introduced from the inlet of the device. Pressured at ~0.5 psi, the growth medium flowed actively through a channel at the flow rate of 20–50 μm/s. The microfluidic device was fixed onto a motorized microscope stage equipped with autofocus (Proscan II, Prior) in a fluorescent microscope (Nikon TI-U) that were housed in a microscope incubator (InVivo Scientific). After 3–4 generations of unperturbed growth at 37°C in the growth chambers, the pressure in the inlet was increased to 3–4 psi to introduce an active flow in the chambers and wash most of the cells out of the chambers. When only a few cells were left in each chamber, the pressure was removed. Then, −0.5 to −1.5 of vacuum was applied from the outlet to bring down the ceiling of the growth chambers and loosely sandwich the trapped cells (side view). Since the vacuum induces the fresh medium flow in a channel (flow rate of 50–100 μm/s), no additional pressure was applied from the inlet. The 20–40 positions that contain a single cell in the view (~100 μm × ~100 μm) of charge-coupled device (CCD) camera (Clara, Andor) with a 60× phase-contrast objective were saved in the motorized stage. Phase-contrast images of the growing cells for each position were recorded two times per doubling. Fluorescence images were taken once per doubling, immediately after phase-contrast images for each position with a Xenon excitation lamp (Sutter Inst.). The images were analyzed with a custom-built Matlab program. First, the program identified pixel positions occupied by cells with phase-contrast images, obtained a size of a growing colony in time series for each position and calculated the growth rate of the colony. In order to get fluorescence levels, fluorescence intensities over the cell-occupying area identified by phase-contrast images were averaged.

Supplementary information

Supplementary information is available at the *Molecular Systems Biology* website (www.nature.com/msb).

Acknowledgements

We are grateful to Sydney Kustu for extensive advice and encouragement throughout this research, and to Jason Hall, Peter Lenz, Jilong Wang and Mike Merrick for discussions. MK also acknowledges Mark Polinkovsky and Edgar Gutierrez for their help with the fabrication of microfluidic chambers. This work was supported by the NIH through grant (R01-GM038361) to Sydney Kustu, the Human Frontiers in Science Program (RGP0022), and by the NSF through grant PHY-1058793 to TH.

Author contributions: MK, DY, AG and TH designed research; MK and HO performed the experiments; MK and TH developed the models and analyzed the data; ZZ constructed strains; MK and TH wrote the paper with contribution from all.

Conflict of interest

The authors declare that they have no conflict of interest.

References

Alibhai M, Villafranca JJ (1994) Kinetic and mutagenic studies of the role of the active site residues Asp-50 and Glu-327 of Escherichia coli glutamine synthetase. *Biochemistry* **33:** 682–686

Andrade SLA, Einsle O (2007) The Amt/Mep/Rh family of ammonium transport proteins. *Mol Membr Biol* **24:** 357–365

Atkinson MR, Blauwkamp TA, Bondarenko V, Studitsky V, Ninfa AJ (2002) Activation of the glnA, glnK, and nac promoters as Escherichia coli undergoes the transition from nitrogen excess growth to nitrogen starvation. *J Bacteriol* **184:** 5358–5363

Blauwkamp TA, Ninfa AJ (2003) Antagonism of PII signalling by the AmtB protein of Escherichia coli. *Mol Microbiol* **48:** 1017–1028

Boussiba S, Dilling W, Gibson J (1984) Methylammonium transport in Anacystis nidulans R-2. *J Bacteriol* **160:** 204–210

Commichau FM, Forchhammer K, Stulke J (2006) Regulatory links between carbon and nitrogen metabolism. *Curr Opin Microbiol* **9:** 167–172

Coutts G, Thomas G, Blakey D, Merrick M (2002) Membrane sequestration of the signal transduction protein GlnK by the ammonium transporter AmtB. *EMBO J* **21:** 536–545

Doucette CD, Schwab DJ, Wingreen NS, Rabinowitz JD (2011) Alpha-ketoglutarate coordinates carbon and nitrogen utilization via enzyme I inhibition. *Nat Chem Biol* **7:** 894–901

Fong RN, Kim KS, Yoshihara C, Inwood WB, Kustu S (2007) The W148L substitution in the Escherichia coli ammonium channel AmtB increases flux and indicates that the substrate is an ion. *Proc Natl Acad Sci USA* **104:** 18706–18711

Groisman A, Lobo C, Cho HJ, Campbell JK, Dufour YS, Stevens AM, Levchenko A (2005) A microfluidic chemostat for experiments with bacterial and yeast cells. *Nat Methods* **2:** 685–689

Gruswitz F, O'Connell J, Stroud RM (2007) Inhibitory complex of the transmembrane ammonia channel, AmtB, and the cytosolic regulatory protein, GlnK, at 1.96 A. *Proc Natl Acad Sci USA* **104:** 42–47

Hirschman J, Wong PK, Sei K, Keener J, Kustu S (1985) Products of nitrogen regulatory genes ntrA and ntrC of enteric bacteria activate glnA transcription *in vitro*: evidence that the ntrA product is a sigma factor. *Proc Natl Acad Sci USA* **82:** 7525–7529

Ikeda TP, Shauger AE, Kustu S (1996) Salmonella typhimurium apparently perceives external nitrogen limitation as internal glutamine limitation. *J Mol Biol* **259:** 589–607

Javelle A, Severi E, Thornton J, Merrick M (2004) Ammonium sensing in Escherichia coli. Role of the ammonium transporter AmtB and AmtB-GlnK complex formation. *J Biol Chem* **279:** 8530–8538

Jiang P, Peliska JA, Ninfa AJ (1998a) Enzymological characterization of the signal-transducing uridylyltransferase/uridylyl-removing enzyme (EC 2.7.7.59) of Escherichia coli and its interaction with the PII protein. *Biochemistry* **37:** 12782–12794

Jiang P, Peliska JA, Ninfa AJ (1998b) Reconstitution of the signal-transduction bicyclic cascade responsible for the regulation of Ntr gene transcription in Escherichia coli. *Biochemistry* **37:** 12795–12801

Jiang P, Peliska JA, Ninfa AJ (1998c) The regulation of Escherichia coli glutamine synthetase revisited: Role of 2-ketoglutarate in the regulation of glutamine synthetase adenylylation state. *Biochemistry* **37:** 12802–12810

Kingdon HS, Shapiro BM, Stadtman ER (1967) Regulation of glutamine synthetase. 8. ATP: glutamine synthetase adenylyltransferase, an enzyme that catalyzes alterations in regulatory properties of glutamine synthetase. *Proc Natl Acad Sci USA* **58:** 1703–1710

Kleiner D (1985) Bacterial ammonium transport. *FEMS Microbiol Rev* **32:** 87–100

Leigh JR (2004) *Control Theory*. Institution of Electrical Engineers, London, UK

Loque D, von Wiren N (2004) Regulatory levels for the transport of ammonium in plant roots. *J Exp Bot* **55:** 1293–1305

Lyons E, Freeling M, Kustu S, Inwood W (2011) Using genomic sequencing for classical genetics in E. coli K12. *PLoS ONE* **6:** e16717

Meek TD, Villafranca JJ (1980) Kinetic mechanism of Escherichia coli glutamine synthetase. *Biochemistry* **19:** 5513–5519

Muro-Pastor MI, Reyes JC, Florencio FJ (2001) Cyanobacteria perceive nitrogen status by sensing intracellular 2-oxoglutarate levels. *J Biol Chem* **276:** 38320–38328

Neidhardt FC, Bloch PL, Smith DF (1974) Culture medium for enterobacteria. *J Bacteriol* **119:** 736–747

Okano H, Hwa T, Lenz P, Yan D (2010) Reversible adenylylation of glutamine synthetase is dynamically counterbalanced during steady state growth of Escherichia coli. *J Mol Biol* **404:** 522–536

Radchenko MV, Thornton J, Merrick M (2010) Control of AmtB-GlnK complex formation by intracellular levels of ATP, ADP, and 2-oxoglutarate. *J Biol Chem* **285:** 31037–31045

Rees AP, Woodward EMS, Joint I (2006) Concentrations and uptake of nitrate and ammonium in the Atlantic ocean between 60 degrees N and 50 degrees S. *Deep Sea Res Part II Top Stud Oceanogr* **53:** 1649–1665

Reitzer L (2003) Nitrogen assimilation and global regulation in Escherichia coli. *Annu Rev Microbiol* **57:** 155–176

Reitzer LJ, Magasanik B (1986) Transcription of glnA in Escherichia coli is stimulated by activator bound to sites far from the promoter. *Cell* **45:** 785–792

Simon SA, Gutknecht J (1980) Solubility of carbon dioxide in lipid bilayer membranes and organic solvents. *Biochim Biophys Acta* **596:** 352–358

Soupene E, He LH, Yan DL, Kustu S (1998) Ammonia acquisition in enteric bacteria: Physiological role of the ammonium/methylammonium transport B (AmtB) protein. *Proc Natl Acad Sci USA* **95:** 7030–7034

Soupene E, Lee H, Kustu S (2002) Ammonium/methylammonium transport (Amt) proteins facilitate diffusion of NH_3 bidirectionally. *Proc Natl Acad Sci USA* **99:** 3926–3931

Soupene E, van Heeswijk WC, Plumbridge J, Stewart V, Bertenthal D, Lee H, Prasad G, Paliy O, Charernnoppakul P, Kustu S (2003) Physiological studies of Escherichia coli strain MG1655: growth defects and apparent cross regulation of gene expression. *J Bacteriol* **185:** 5611–5626

Truan D, Huergo LF, Chubatsu LS, Merrick M, Li XD, Winkler FK (2010) A new P(II) protein structure identifies the 2-oxoglutarate binding site. *J Mol Biol* **400:** 531–539

Walter A, Gutknecht J (1986) Permeability of small nonelectrolytes through lipid bilayer membranes. *J Membr Biol* **90:** 207–217

Woolfolk CA, Stadtman ER (1964) Cumulative feedback inhibition in multiple end product regulation of glutamine synthetase activity in Escherichia coli. *Biochem Biophys Res Commun* **17:** 313–319

Woolfolk CA, Stadtman ER (1967) Regulation of glutamine synthetase 3. Cumulative feedback inhibition of glutamine synthetase from Escherichia coli. *Arch Biochem Biophys* **118:** 736–755

Wulff K, Mecke D, Holzer H (1967) Mechanism of enzymatic inactivation of glutamine synthetase from E. coli. *Biochem Biophys Res Commun* **28:** 740–745

Yan D, Lenz P, Hwa T (2011) Overcoming fluctuation and leakage problems in the quantification of intracellular 2-oxoglutarate levels in Escherichia coli. *Appl Environ Microbiol* **77:** 6763–6771

Yuan J, Doucette CD, Fowler WU, Feng XJ, Piazza M, Rabitz HA, Wingreen NS, Rabinowitz JD (2009) Metabolomics-driven quantitative analysis of ammonia assimilation in E. coli. *Mol Syst Biol* **5:** 16